RESEARCH ARTICLE

Spectroscopic and electrokinetic evidence for a bifunctional mechanism of the oxygen evolution reaction

Lichen Bai,[a, ‡] Seunghwa Lee,[a, ‡] and Xile Hu*[a]

[a] L. Bai, Dr, S. Lee, Prof. X. Hu
Laboratory of Inorganic Synthesis and Catalysis, Institute of Chemical Sciences and Engineering, ISIC-LSCI
École Polytechnique Fédérale de Lausanne (EPFL)
1015 Lausanne, Switzerland
E-mail: xile.hu@epfl.ch Homepage: http://lsci.epfl.ch
‡ These authors contributed equally.

Supporting information for this article is given via a link at the end of the document.

Abstract: The oxygen evolution reaction (OER) is an essential anodic reaction in many energy storage processes. OER is most often proposed to occur via a mechanism involving four consecutive proton-coupled electron transfer (PCET) steps, which imposes a performance limit due to the scaling relationship of various oxygen intermediates. A bifunctional OER mechanism, in which the energetically demanding step of the attack of hydroxide on a metal oxo unit is facilitated by a hydrogen atom transfer to a second site, has the potential to circumvent the scaling relationship. However, the bifunctional mechanism has hitherto only been supported by theoretical computations. Here we describe an operando Raman spectroscopic and electrokinetic study of two highly active OER catalysts, FeOOH-NiOOH and NiFe layered double hydroxide (LDH). The data support two distinct mechanisms for the two catalysts: FeOOH-NiOOH operates by a bifunctional mechanism where the rate-determining O-O bond forming step is the OH^- attack on a Fe=O coupled with a hydrogen atom transfer to a Ni^{III}-O site, whereas NiFe LDH operates by a conventional mechanism of four consecutive PCET steps. The experimental validation of the bifunctional mechanism enhances the understanding of OER catalysts.

Introduction

The oxygen evolution reaction (OER) is an essential anodic reaction for many cathodic electrochemical reactions, such as hydrogen evolution reaction (HER), CO_2 reduction reaction (CRR), and N_2 reduction reaction (NRR), which may be used to generate renewable fuels and valuable chemicals.[1] An electrocatalyst, typically a metal oxide or oxyhydroxide, is required for OER to occur at a conceivable rate.[2] The OER involves four electrons and protons, rending it mechanistically complex.[2a, 2c, 3] For OER catalyzed by metal oxides and oxyhydroxides, the most commonly assumed mechanism involves four consecutive proton-coupled electron transfer, where the O-O bond forming step is nucleophile attack of water or hydroxide on a metal oxo species (Scheme 1a).[3a, 4] DFT computations revealed a scaling relationship between the adsorption energies of OH*, O*, and OOH*.[4-5] In particular, the difference of the adsorption energies of *OH and *OOH is always 3.2 eV for nearly all metal oxides. This scaling relationship poses an upper limit on the performance of OER catalysts, which has a theoretical overpotential of about 0.4 eV.[4-5]

To break the performance limit imposed by the scaling relationship, a change of catalytic mechanism is required.[6] An alternative mechanism involves the combination of two metal oxo species as the O-O bond forming step (Scheme 1b). Although there is theoretical debate in whether this O-O bond forming step is kinetically favourable compared to the nucleophilic attack step,[7] electrokinetic studies seem to support such a mechanism in a number of systems.[8] In addition to these two conventional mechanisms, a third-type, so-called “bifunctional” mechanism has recently been proposed.[6b, 9] This mechanism involves two catalytic sites, often based on two different metal ions, which work in a cooperative manner (Scheme 1c). One site provides the electrophilic M=O entity, while the other side provides a hydrogen atom acceptor (A). Although the direct nucleophilic attack of an OH^- on the M=O to form the M-OOH intermediate is energetically too unfavourable, a concerted hydrogen atom transfer to the neighbouring acceptor significantly lowers the energetics.

Until now, the bifunctional mechanism is supported by DFT computations only.[6b, 9] In a previous study, we developed an unconventional iron nickel catalyst, FeOOH-NiOOH, that was significantly more active than Ni-Fe oxyhydroxides and related layered double hydroxides ($NiFeO_xH_y$ and NiFe LDH), which were the benchmark OER catalyst in alkaline medium.[9c] Operando X-ray absorption spectroscopy revealed the catalyst as nanoclusters of γ-FeOOH covalently linked to a γ-NiOOH support. According to DFT computations, this structure could enable a bifunctional mechanism where the O-O bond forming step is a nucleophilic attack of OH^- on a Fe=O moiety coupled with a concerted hydrogen atom transfer to a nearby terrace O site on the γ-NiOOH support. Here we present in-situ Raman spectroscopy and electrokinetic data that support this mechanism. The experimental validation of the bifunctional mechanism stimulates both the mechanistic understanding and the design principles of OER catalysts.

Results

Compositions and activity of catalysts

As described previously, FeOOH-NiOOH was prepared by dipping a clean nickel form (NF) in a solution of $FeCl_3$, drying in air at 80 °C, followed by anodic activation in a Fe-containing KOH.[9c] While previously we assigned the support as pure NiOOH, we found in the present study that some Fe ions were incorporated in the lattice of NiOOH, which resulted in a positive

shift of the $Ni(OH)_2$/NiOOH oxidation potential[10] during the formation of FeOOH-NiOOH (Figure S1). The distribution of Fe was not uniform, according to transmission electron microscopy (TEM), and energy dispersed X-ray (EDX) mapping (Figure S2 and S3). Because Fe-doped NiOOH is an active OER catalyst,[10] to probe the possible influences of the Fe doping in the NiOOH support in the activity and mechanism, we chose NiFe LDH as a reference sample. Previous studies suggested the structure of NiFe LDH is the active motif of Fe-doped NiOOH.[10a, 11] Additionally, DFT computations suggested OER occurred via four consecutive PCET steps on this conventional NiFe oxyhydroxide catalyst.[11-12] The NiFe LDH was prepared according to literature.[13] The compound was characterized by powdered X-ray diffraction (PXRD), transmission electron microscopy (TEM), and energy dispersed X-ray (EDX) mapping (Figure S4 and S5). The Ni and Fe ions appeared to be uniformly distributed in NiFe LDH (Figure S5), and the Fe content was about 22%.

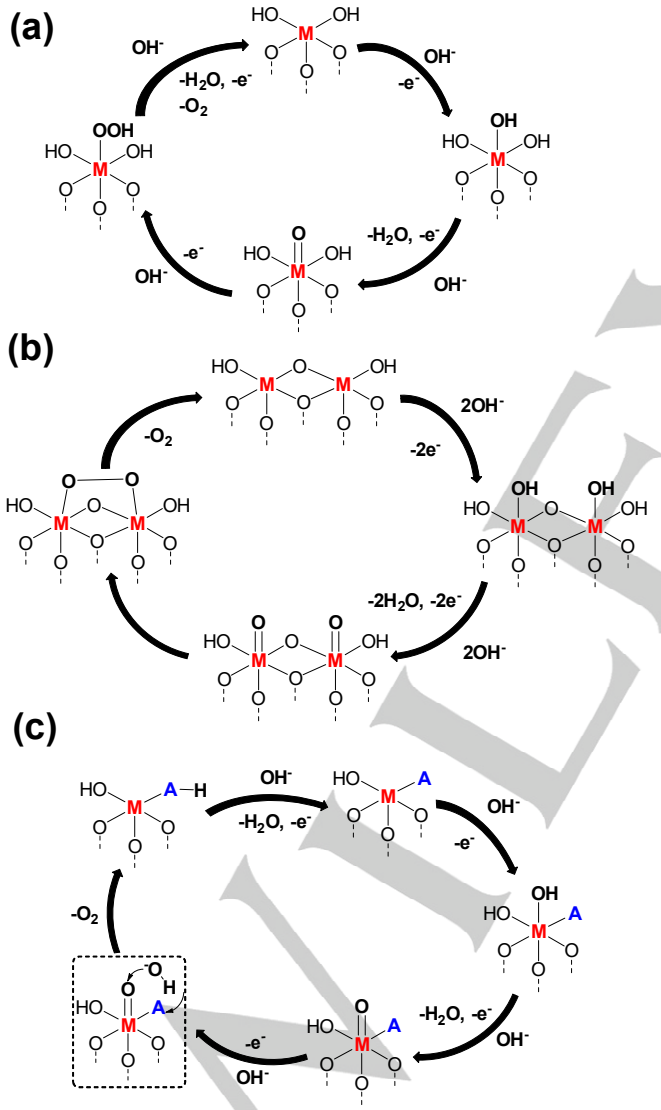

Scheme 1. Three OER mechanisms in alkaline conditions. (a) A conventional mechanism involving four consecutive proton-coupled electron transfers; (b) A conventional mechanism involving combination of two metal oxo species as the O-O bond forming step; (c) An unconventional 'bifunctional' mechanism. M represents an active metal center, and A represents a hydrogen atom acceptor.

We compared the activity of FeOOH-NiOOH and NiFe LDH with similar Fe loadings after electrochemical activation (Figure S6). To avoid the formation of some FeOOH-NiOOH on NF during OER test,[9c] the activity of NiFe LDH was tested on a carbon-cloth (CC) electrode. Both catalysts were activated by multiple cyclic voltammetric (CV) scans (Figure S1a, S7). The activation of FeOOH-NiOOH was related to the incorporation of Fe ions and formation of FeOOH as reported previously.[9c] The activation of NiFe LDH was related to a morphology change that increased the surface area, which was indicated by the increase of areas of the oxidation of $Ni(OH)_2$ to NiOOH (Figure S7). Moreover, TEM and HAADF-STEM images (Figure S4b, S5, S8 and S9) showed that the initial, large lamellar structure cracked into small layers upon activation, while the Fe/(Ni+Fe) ratio remained unchanged (Figure S5e, S6c and S9e). According to linear sweep voltammetry (LSV) data (Figure 1a and S10), the FeOOH-NiOOH is significantly more active than NiFe LDH, both in apparent geometric activity (Figure 1a) and in double-layer capacitance normalized activity (Figure S10). The turnover frequencies (TOFs) were also compared assuming a bimetallic Ni-Fe active site for both catalysts (Figure 1b). The FeOOH-NiOOH has TOFs that are about 10 times higher than those of NiFe LDH. These data indicate a difference in the active sites of FeOOH-NiOOH and NiFe LDH, and confirm that the Fe-doped NiOOH support had no noticeable contribution to the measured activity of FeOOH-NiOOH.

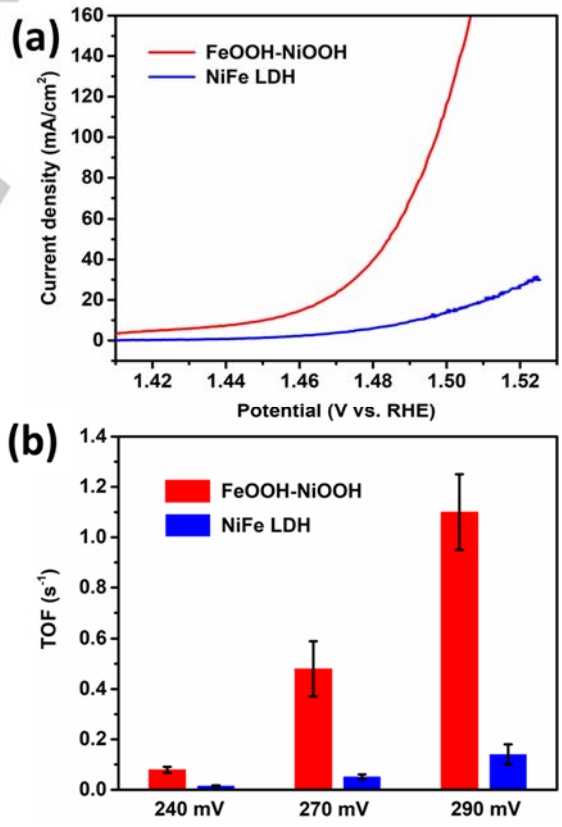

Figure 1. Electrocatalytic activity. (a) LSV curves of FeOOH-NiOOH (red) and NiFe LDH (blue) in 1 M KOH. (b) Comparison of TOFs of FeOOH-NiOOH on NF (red) and NiFe LDH on carbon cloth (blue) at various overpotentials.

Operando Raman spectroscopic data

Figure 2 shows operando Raman optical microscopy images and spectra of FeOOH-NiOOH, recorded from the open circuit potential (OCP) to 1.6 V (vs. RHE) with an interval of 0.1 V. Due to FeOOH, the surface looks brownish-yellow at OCP compared with bare NF (Figure S11), which is silver-white.[9c, 14] The microscope objective collected Raman signals from three different beam spots (I, II, and III in Figure 2a). The surface gradually turned into black from 1.4 V (Figure 2b-f), indicative of the formation of Fe-doped NiOOH support.[15] The potential-dependent Raman spectra vary at three different spots of the surface (Figure 2g-i), indicating a surface heterogeneity. Indeed TEM and EDX mapping images (Figure S2 and S3) showed that Fe ions were not uniformly distributed on the surface. Consistent with previous XAS results,[9c] surface γ-FeOOH species were identified by two main Raman bands at 526 cm^{-1} and 690 cm^{-1} (Figure 2g-i and S12).[9c, 16] At 1.4 V and above, two strong Raman bands at around 480 and 560 cm^{-1} were observed (Figure 2g-i). These two bands correspond to the Ni-O bending and stretching vibrations of NiOOH, respectively.[10c, 17] Their appearance indicated the presence of NiOOH at these potentials, again consistent with previous XAS data.[9c] Control experiments showed that the Raman specta of bare FeOOH are identical from OCP to 1.8 V (Figure S13). Nevetheless, the Raman peaks of FeOOH in FeOOH-NiOOH become invisible due to overlapping with the strong bands of NiOOH at 1.4 V and above (Figure 2g-i). At the three chosen spots on the surface of FeOOH-NiOOH, the relative intensities of the 480 cm^{-1} and 560 cm^{-1} bands (I_B/I_S) and the half-widths of the two bands vary, indicating different local environments around the Ni-O bonds. Fe-incorporation into NiOOH causes structural defects and disorder of lattice, which leads to a lower I_B/I_S.[10c, 17a, 17d] Accordingly, the amount of Fe dopant in the NiOOH at the three spots follows the order of: III > I > II. A broad band in the frequency range of 900 to 1150 cm^{-1}, previously attributed to Ni-OO^-,[17a-c, 18] was observed from 1.375 V (Figure S14a).

A previous study reported that FeOOH was not a stable OER catalyst in alkaline medium and would be dissolved at high overpotentials.[19] We found that the Fe loadings of FeOOH-NiOOH indeed decreased after activation by multiple CVs (Figure S6b). However, after activation both the Fe loading and OER activity remained stable in an 18 h electrolysis at 10 mA/cm^2 (Figure S6b and S15a). The Raman spectra were measured after 1 h, 2 h, 3 h and 18 h of constant current electrolysis, showing no obvious changes of the peaks associated with γ-FeOOH (Figure S15b). The improved stability of FeOOH in FeOOH-NiOOH compared to bare FeOOH is probably due to the covalent interaction with the NiOOH substrate.

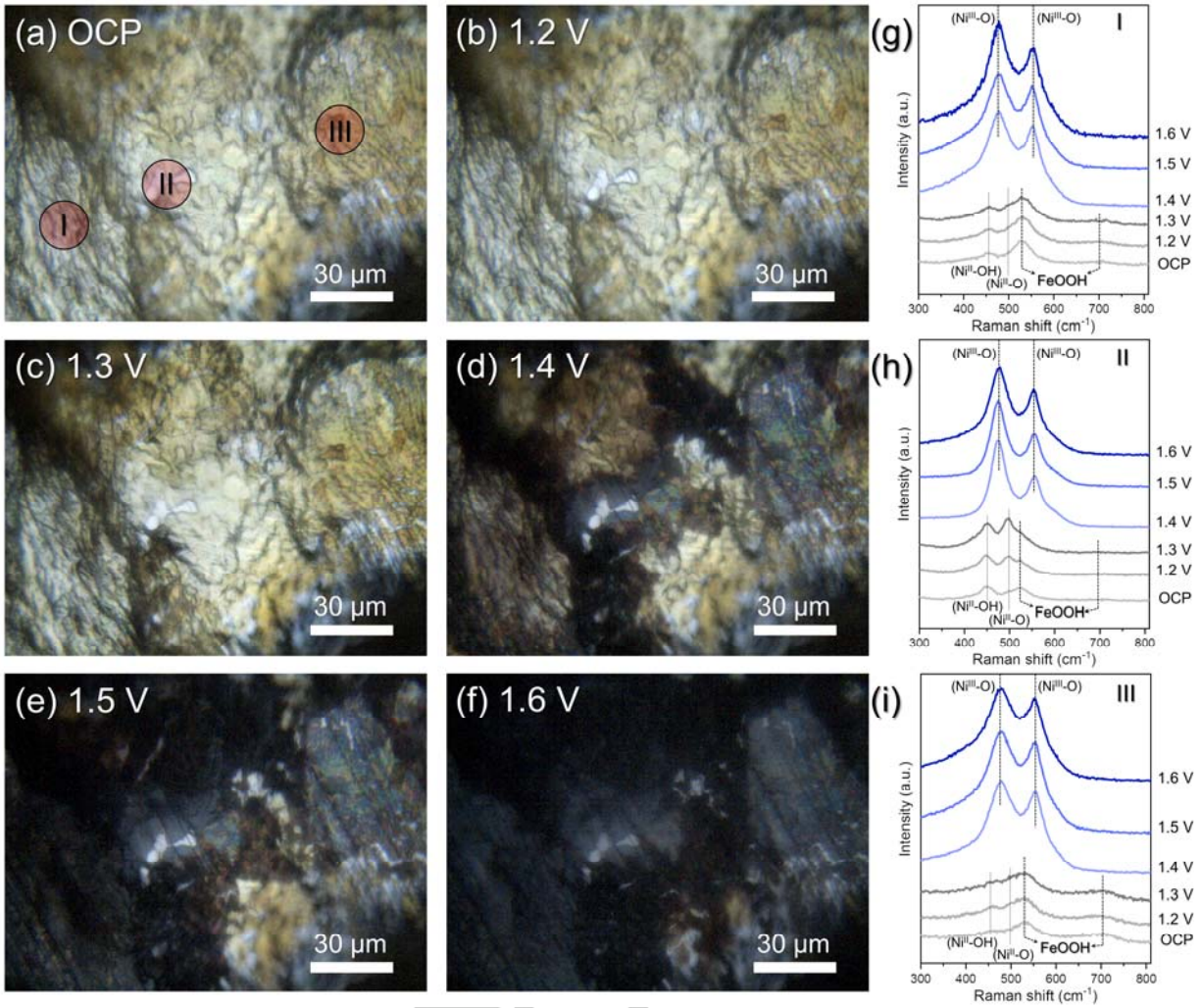

Figure 2. Operando Raman spectroscopic analysis. (a-f) Optical microscopy images of FeOOH-NiOOH at given potentials and (g-i) the corresponding operando Raman spectra obtained from three different spots as indicated in the (a).

The Operando Raman spectra collected of NiFe LDH from OCP to 1.5 V (Figure S14b) show no spectral features corresponding to γ-FeOOH. Compared to Ni hydroxide and pure NF, NiFe LDH exhibits a peak corresponding to Ni^{II}-O vibration at around 525 cm^{-1} but not 500 cm^{-1}, which originates from the structural disorder induced by Fe doping. (Figure S14b and S16).[16a, 17d, 20] The two Raman bands of Ni^{III}-O (from NiOOH) began to grow from 1.375 V and the growth was completed at around 1.45 V (Figure S14b). The broad band in higher frequency range of 900 to 1150 cm^{-1}, due to Ni-OO^-,[17a-c, 18] appeared from about 1.4 V.(Figure S14b).

We compare directly the representative Raman spectra of FeOOH-NiOOH and NiFe LDH at OCP and 1.5 V (Figure S17). At OCP, Ni is mostly in the +2 oxidation state, and the Ni^{II}-O bands have low intensities (Figure S17, left). Accordingly, Raman bands due to FeOOH could be observed (Figure S17, left). The presence of FeOOH in FeOOH-NiOOH, but not NiFe LDH, was obvious. At 1.5 V, NiOOH is formed where Ni is in the oxidation state of +3, and the Ni^{III}-O bands have high intensities (Figure S17, right). The I_B/I_S of NiFe LDH (1.18) was significantly lower than that of FeOOH-NiOOH (1.72), bare NF (1.91), and Ni hydroxide (2.2) (Figure S17 and S18), indicative of the highest structural disorder of NiFe LDH among the four samples. Because this NiFe LDH sample contains 20% whereas FeOOH-NiOOH has an Fe content of about 10% in some region (Figure S3), Raman spectra were also recorded for a NiFe LDH with 10% Fe (Figure S19, EDX mapping images and CVs of this catalyst are in Figure S20-S21). The I_B/I_s of NiFe LDH (10%Fe) was 1.33, again lower than that of FeOOH-NiOOH.

We conducted ^{18}O isotope labeling and exchange experiments on FeOOH-NiOOH and NiFe LDH. The as-prepared, ^{16}O-labeled, samples were first immersed in a ^{18}O-KOH solution. For FeOOH-NiOOH at OCP to about 1.3 V, the peak of FeOOH remained at the same position whereas the peaks of Ni^{II}-O, Ni^{II}-OH appeared to be shifted, but the shift could not be quantified due to an overlap of peaks.(Figure 3a, left) For NiFe LDH same as reported previously,[17a, 17b] the peaks of Ni^{II}-O, Ni^{II}-OH at OCP to about 1.35 V red-shifted by about 22 cm^{-1}, indicating the exchange of lattice ^{16}O with ^{18}O of the electrolyte (Figure 3a, right). Upon formation of NiOOH, and more obviously at 1.55 V, the Ni^{III}-O bands were observed at around 455 and 535 cm^{-1} for both FeOOH-NiOOH and NiFe LDH, red-shifted by about 22 cm^{-1} relative to those of ^{16}O-labeled samples. This shift indicates O isotope exchange. For FeOOH-NiOOH, the Raman peaks of γ-FeOOH did not shift during this process up to 1.325 V. At higher potentials the peaks were hidden by those of Ni^{III}-O bands. To probe whether lattice O in FeOOH was exchanged during OER, a FeOOH-NiOOH sample was first subjected to a ^{18}O-KOH solution at 1.55 V where OER was occurring, and then the Raman spectrum was collected at 1.25 V. Again the Raman peaks of γ-FeOOH remained at the same positions of a ^{16}O-labeled sample (Figure S22). Thus, the lattice oxygens of γ-FeOOH do not exchange with the electrolyte even under OER.

The ^{18}O-labeled samples of FeOOH-NiOOH and NiFe LDH were immediately placed back in a 1 M ^{16}O-KOH solution and potentiostatically charged at 1.55 V. For FeOOH-NiOOH, the peaks corresponding to Ni^{III}-O vibrational modes were shifted by about 3 cm^{-1} to high frequencies (Figure 3b, left). For NiFe LDH, no shift of peaks related to Ni^{III}-O was observed (Figure 3b, right). As a reference, a shift of 18 cm^{-1} was observed on bare NF (Figure S23).

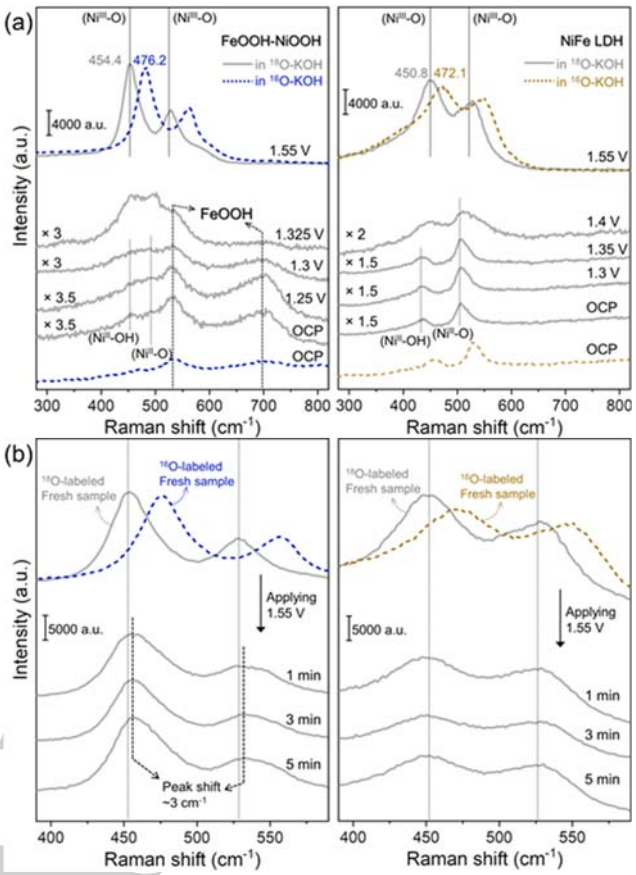

Figure 3. Operando Raman spectra of FeOOH-NiOOH (left column) and NiFe LDH (right column) obtained at various potentials for oxygen isotope labeling (a) in 1 M KOH-$H_2{}^{18}O$ solution and (b) subsequent isotope exchange experiments. The ^{18}O-labeled samples were monitored at 1.55 V in 1 M KOH-$H_2{}^{16}O$ solution. For ease of comparison of peak shift in between the two solutions, ^{16}O-labeled peaks of each sample are indicated respectively.

Electrokinetic data

FeOOH-NiOOH exhibited a similar Tafel Slope of 38±2 mV/dec in 0.5 M to 2 M KOH (Figure 4a, S24a, Table S1). The potentials vs. Ag/AgCl (pH independent) at 10 mA/cm^2 linearly depended on the log of the concentration of hydroxyl ions (Figure 4b), with a slope of -74 mV/dec. The rate order of [OH^-] in 0.5-2 M KOH was determined according to [Eq. (1)].

$$\left(\frac{\partial \log j}{\partial \log [OH^-]}\right)_E = -\frac{\left(\frac{\partial E}{\partial \log [OH^-]}\right)_j}{\left(\frac{\partial E}{\partial \log j}\right)_{pH}} \qquad (1)$$

The denominator of [Eq. (1)] is the Tafel slope and the numerator is the slope in Figure 4b. Accordingly, the order of [OH^-] was 1.8±0.1.

Similar analysis was performed for NiFe LDH (Figure 4c, 4d, S25a). The Tafel slopes of NiFe LDH are 42 to 48 mV/dec, depending on the concentration of hydroxyl ions (Figure 4c, Table S1). The Tafel slope decreased with increasing [OH^-]. The Tafel slope in 2 M KOH is close to 40 mV/dec, similar to that of FeOOH-NiOOH. The potentials vs. Ag/AgCl (pH independent) at 1 mA/cm^2 linearly depended on the log of the concentration of hydroxyl ions (Figure 4d), with a slope of -80 mV/dec. According to [Eq. (1)], the rate order of [OH^-] was also close to two.

The redox potentials of the precatalytic Ni(II)/Ni(III) shifted negatively by ca. 100 mV when the [OH^-] increased by 10 fold, indicating a $3OH^-/2e^-$ process (Figure S24b-c, S25b-c) for both

FeOOH-NiOOH and NiFe LDH. The activity of NiFe LDH was very different in 1 M KOH, NaOH, LiOH (Figure S26a), indicating a cation effect. On the contrary, the cation effect was not obvious for FeOOH-NiOOH (Figure S26b).

The OER activity of FeOOH-NiOOH had an H/D isotope effect of 1.4 to 2.0, depending on the concentration of hydroxyl ions and the applied potential (Figure 4e, S27a, S28a). On the other hand, NiFe LDH had an H/D isotope effect of 2.0-2.4 (Figure 4f, S27b, S28b), and the isotope effect did not vary substantially at different potentials nor [OH^-].

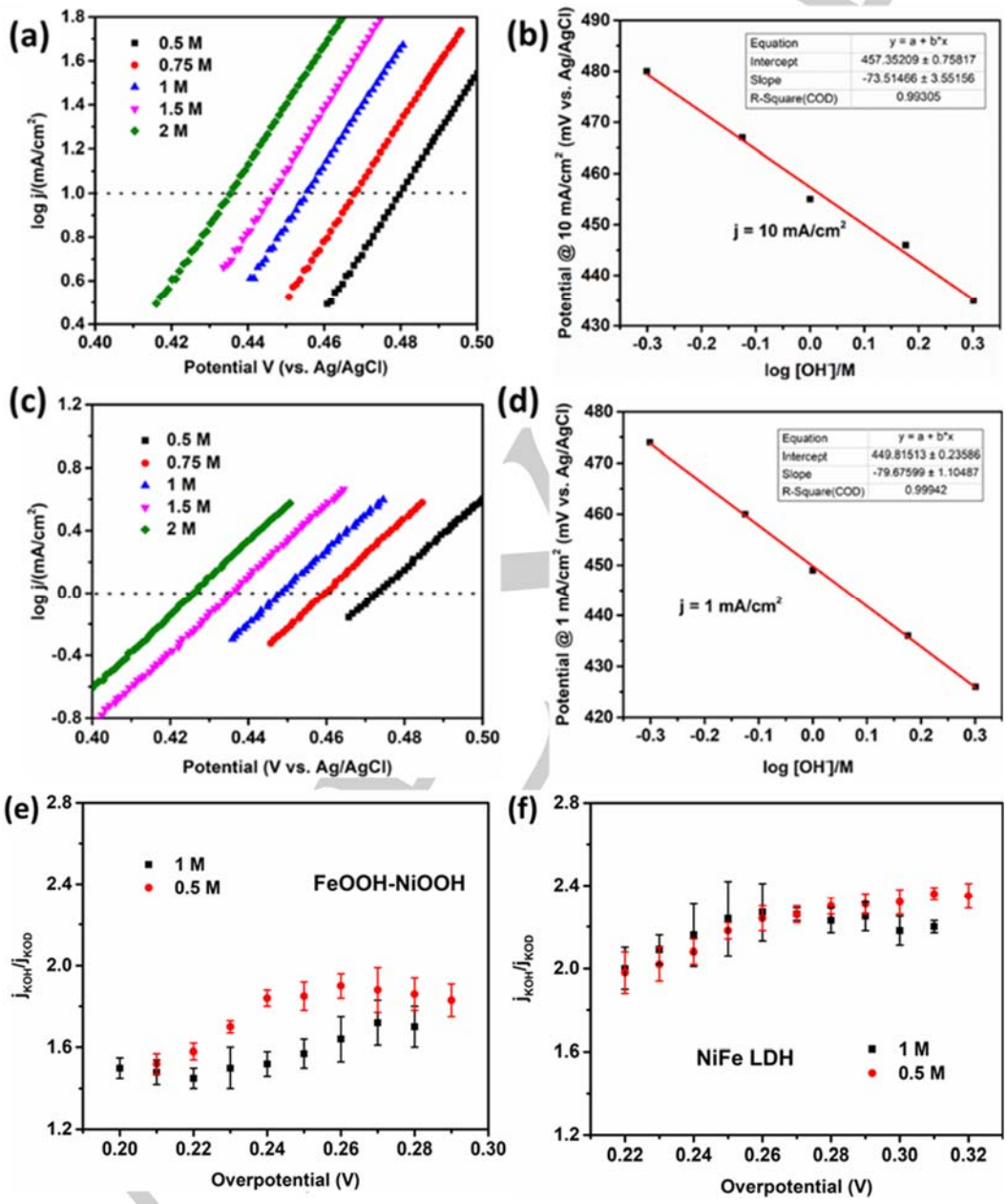

Figure 4. Electrokinetic analysis. (a) and (b) for FeOOH-NiOOH. (c) and (d) for NiFe-LDH. (a) and (c) The Tafel plots in different concentrations of KOH. The original LSVs are provided in SI. (b) and (d) The change of constant potential at a certain current density (10 mA/cm^2 for FeOOH-NiOOH and 1 mA/cm^2 for NiFe LDH) based on the logarithm of [OH^-]. The linear fitting of the data points gives the $(\partial E/\partial \log [OH^-])_j$ values, as the slope of the fitting plot. (e-f) H/D isotope effect analysis (j_{KOH}/j_{KOD} versus overpotential). (e) NiFe LDH and (f) FeOOH-NiOOH. Electrolyte concentrations: 1 M (black), 0.5 M (red). The error bar and the average values were deduced from 3 independent measurements.

Discussion

Raman spectroscopic analysis

Operando Raman spectra revealed the presence of surface γ-FeOOH in FeOOH-NiOOH, but not in NiFe LDH. Otherwise the two catalysts have a similar component, Fe-doped γ-NiOOH. Bulk γ-FeOOH is a poor OER catalyst,[11, 19] whereas the surface γ-FeOOH here is responsible for remarkable OER activity (Figure 1, and S10). This difference suggests a mechanism that involves more than γ-FeOOH alone. The doping of Fe in NiOOH causes structural disorder in the lattice of NiOOH, which could be inferred by the I_B/I_S of the Raman spectra of NiOOH. [10c, 17a, 17d] The lower structural disorder of FeOOH-NiOOH compared to NiFe LDH is consistent with most Fe ions being on the surface in FeOOH-NiOOH but in the bulk of NiFe LDH.

As reported previously,[17a, 17b] the lattice O of NiOOH in NiFe LDH can exchange with O from the OH^- electrolyte. The exchange can occur without applying a potential when Ni is at the +2 oxidation state (as in $Ni(OH)_2$), but not when Ni is oxidized to +3 or above. The lattice O of NiOOH in FeOOH-NiOOH can also be exchanged at the Ni^{II} stage. Under OER potentials, a 3 cm^{-1} isotopic shift of FeOOH-NiOOH indicates partial O exchange. Compared to bulk NF (18 cm^{-1} shift), the exchange is about 16%. The different O exchange behavior reflects a mechanistic difference between FeOOH-NiOOH and NiFe LDH.

Electrokinetic analysis

We employed a quasi-equilibrium model to describe the OER kinetics, in which the key steps are described by one pre-equilibrium step (PES) plus one rate-determining step (RDS).[21] The RDS limits the OER velocity while the PES determines the concentration of the resting states. The overall OER rate and catalytic behavior are controlled by both steps. The other steps are fast and do not restrict overall reaction rate. This model is suitable for catalysts in the intermediate applied overpotential (Tafel region), where the concentration of the resting state is not high (see Appendix 1, SI).

For the conventional mechanism involving four PCET steps (Scheme 1a), if the formation of M=O is the PES, and the nucleophilic attack of OH^- on a M=O is the RDS (Scheme 1a), the predicted Tafel slope is 40 mV/dec and the predicted rate order in $[OH^-]$ is two, assuming there is no charge transfer barrier.[21b, 22] For the bifunctional mechanism (Scheme 1c), if the formation of M=O is the PES, and the nucleophilic attack of OH^- on a M=O coupled with a hydrogen atom transfer is the RDS (Scheme 1c), the predicted Tafel slope is also 40 mV/dec and the predicted rate order in $[OH^-]$ is also two (Appendix 1, SI). The experimental values for both FeOOH-NiOOH and NiFe LDH, thus, agree with the predictions of both mechanisms. However, there are noticeable differences in the Tafel behaviors of FeOOH-NiOOH and NiFe LDH. The Tafel slopes of FeOOH-NiOOH is independent of $[OH^-]$. In contrast, the Tafel slope of NiFe LDH decreases with increasing $[OH^-]$, suggesting a charge transfer barrier across the bulk film, which is more pronounced at lower $[OH^-]$ (for a detailed description, see SI, Appendix 1).[23] The absence of charge transfer barrier in FeOOH-NiOOH would be consistent with surface-dominated catalysis. The significant cation effect for NiFe LDH also indicates bulk sites are involved in OER,[24] although the origin of this effect is under debate.[24] The small cation effect observed for FeOOH-NiOOH is again consistent with surface catalysis.

H/D exchange affects both thermodynamics and kinetics of PCET reactions.[25] Accordingly, both thermodynamic isotope effect (TIE) and the kinetic isotope effect (KIE) exist.[25] The TIE originates from a change in the reaction thermodynamics due to different vibrational zero-point energies (ZPEs) of bonds involving hydrogen and deuterium.[25a, 26] In the present case, H/D TIE effect should be observed in PES involving proton transfer. On the other hand, H/D KIE originates from the different activation barriers caused by the differences of ZPEs between H- and and D-substituted analogues.[25, 27]. KIE is usually employed to probe the involvement of proton transfer in RDS.[25, 27] The combination of TIE and KIE leads to the overall observed isotope effect (IE).

For the conventional mechanism (Scheme 1a), there is direct proton transfer in the PES but not in RDS. Consequently, only TIE and secondary KIE are expected. Secondary KIE is typically below 1.3,[27a, 28] so TIE would dominate. The data for NiFe LDH (H/D IE of 2.0-2.4) fit this model. The IE is roughly independent of applied potential, characteristic of TIE.[8b, 26] Moreover, the IE is pH-independent, consistent with a PCET-type PES.[8b, 26]

For the bifunctional mechanism, the direct proton/hydrogen transfer is involved in both PES and RDS (Scheme 1c), so that KIE becomes significant. In the Tafel region, the overall IE can be expressed as [Eq. (2)] (Appendix 2 of SI).[27a]

$$IE = \frac{k_0}{k_0'}\exp\left(\frac{(\alpha_2-\alpha_2')\eta F}{RT}\right) \qquad (2)$$

k_0 and k_0' are the rate constants of H- and D-substituted reactants, respectively; α_2 and α_2' are the transfer coefficients of RDS for H- and D-substituted reactants; R, T, η, and F are universal gas constant, thermodynamic temperature, overpotential, Faradaic constant, respectively. Typically α_2 is bigger than α_2' due to a higher barrier of charge transfer after D-substitution.[27a] In the Tafel region, k_0 and k_0', α_2 and α_2' can be considered potential-independent. Therefore, the observed IE should increase with increasing overpotential. Moreover, if the generation of the hydrogen atom acceptor is pH-dependent, the KIE is expected to depend on pH as well.[29] The data for FeOOH-NiOOH fit this model. The observed isotopic effect indeed increases with applied overpotential, and decreases with $[OH^-]$. Note that the overall IE of FeOOH-NiOOH, dominated by KIE, is lower than that of NiFe LDH, dominated by TIE. Accordingly, the TIE of FeOOH-NiOOH is lower than that of NiFe LDH, reflecting a difference in the nature of M=O in these two catalysts. The KIE of FeOOH-NiOOH is rather small likely due to the internal hydrogen transfer in RDS. Previous literatures suggested internal hydrogen or proton acceptor could minimize the H/H^+ transfer distance, significantly decreasing the H/D KIE.[30]

Catalytic cycle

Based on the above data, we propose a catalytic cycle for FeOOH-NiOOH (Figure 5a). The as-prepared catalyst A-I is composed of γ-FeOOH clusters covalently linked to a $Ni(OH)_2$ support, which is lightly doped by Fe. At about 1.35 V, the support is oxidized to NiOOH via a $3OH^-/2e^-$ process. The process is best described by oxidation of a dimeric Ni^{II} unit into a dimeric Ni^{III} unit accompanied by the loss of three protons from coordinated water or OH^- groups (A-II). The Fe^{III} center in FeOOH then undergoes a PCET to form an electrophilic Fe(IV)=O center (A-III), which is the PES of the catalytic cycle. Consequently and in the RDS, the Fe(IV)=O center, an external OH^-, and the Ni^{III}-O moiety react in a concerted manner to give Fe^{II}-Ni^{II}-OH (A-IV), O_2 and an electron. Oxidations of Fe^{II} and Ni^{II} then regenerates the catalyst (A-II).

For NiFe LDH (Figure 5b), the as-prepared catalyst is comprised of $Ni(OH)_2$ doped by Fe^{III} ions (B-I). A $3OH^-/2e^-$ process generates Fe-doped NiOOH (B-II). Although there are debates on whether Ni or Fe site serves as the site of O-O bond formation,[2a, 11, 31] a dimeric Fe-O-Ni active site would agree with most data. The catalytic cycle proceeds via a PES to form a M=O (B-III, assuming M is Fe, but the same result is obtained when M is Ni), followed by a RDS of OH^- attack on M=O to give M-OOH (B-IV). A further PCET oxidation gives O_2 and M (B-V), which can then be oxidized back to the initial catalyst B-II. When M is Fe, the Fe ions shuffle between Fe^{II}, Fe^{III}, and Fe^{IV} while the Ni ions remain as Ni^{III} during catalysis. When M is Ni, the Ni ions shuffle between Ni^{II}, Ni^{III}, and Ni^{IV} while the Fe ions remain as Fe^{III}.

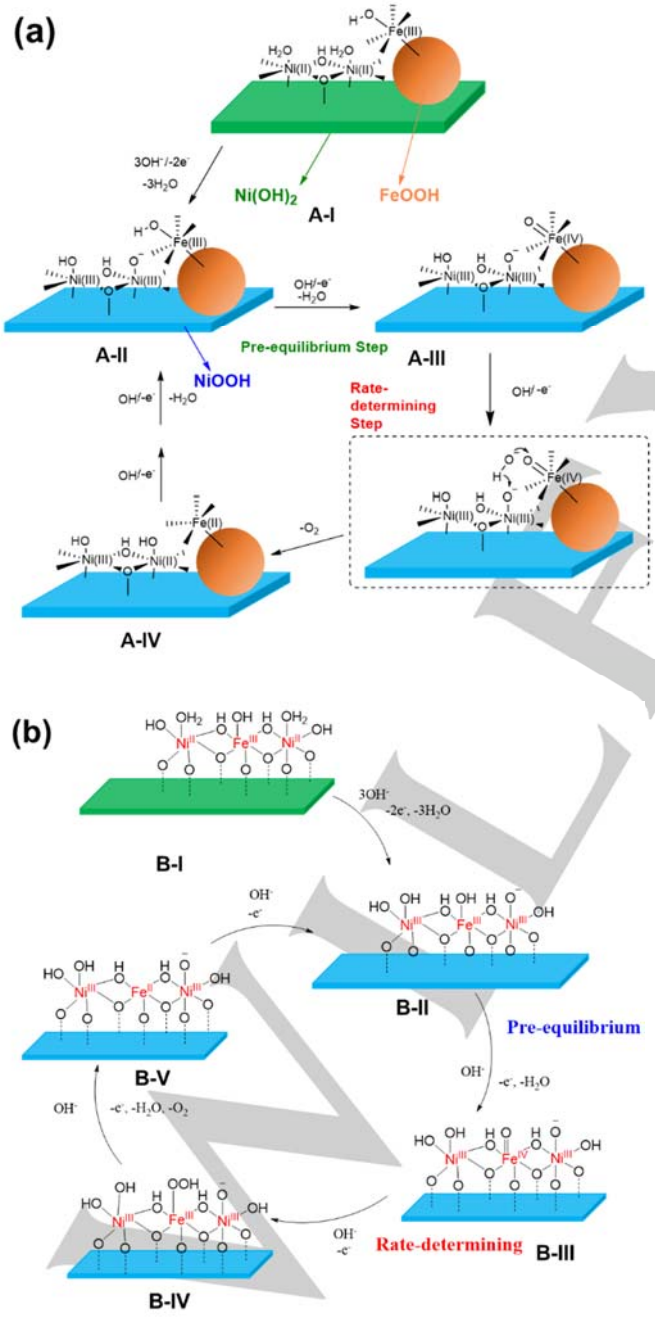

Figure 5. Proposed OER reaction mechanisms of (a) FeOOH-NiOOH. (b) NiFe LDH (assuming Fe is the catalytic center).

The results from O isotope exchange experiments (Figure 3b) suggest the presence of transient Ni^{II} sites in FeOOH-NiOOH but not NiFe LDH during OER. About 16% of lattice O in FeOOH-NiOOH exchanges with OH^- under OER, but such an exchange is absent in NiFe LDH. It is known that at Ni^{II} the lattice O of Fe-doped NiOOH and NiFe LDH can exchange with O from OH^- electrolyte without applied potential, but at Ni^{III} and above, the exchange does not occur even under OER.[17a, 17b] These results are consistent with FeOOH-NiOOH operating via the bifunctional mechanism (Figure 5a) where a Ni^{III}-O site accepts a hydrogen atom in the RDS to become a Ni^{II}-OH site. They are also consistent with NiFe LDH operating via the conventional mechanism (Figure 5b) where the redox changes occur at the Fe site.

Conclusion

Operando Raman spectroscopy and electrokinetic analysis were employed to study two active OER catalysts, FeOOH-NiOOH and NiFe LDH. Despite their similar chemical compositions, the two catalysts exhibit different electrochemical and spectroscopic features, which indicate that most Fe ions exist in surface γ-FeOOH clusters in FeOOH-NiOOH but they are doped in the lattice of $Ni(OH)_2$/NiOOH in NiFe LDH. This different results in a 10-fold higher OER activity of FeOOH-NiOOH compared to NiFe LDH. During OER, different O isotope exchange behaviors of the NiOOH component were observed for the two catalysts: about 16% of lattice O in FeOOH-NiOOH exchanged with the OH^- electrolyte whereas there was no exchange for NiFe LDH. These data suggest that Ni^{II} species are present in the catalytic cycle of FeOOH-NiOOH, but not NiFe LDH. The two catalysts exhibit similar Tafel slopes and rate orders in $[OH^-]$ under standard conditions. However, they have different H/D isotope effects. FeOOH-NiOOH has an IE of 1.4 to 2.0, which had a significant KIE component and depend on $[OH^-]$ and the overpotential. NiFe LDH had an IE of 2.0-2.4, which is mostly TIE and is independent of $[OH^-]$ and the overpotential. The spectroscopic and kinetic data support two distinct mechanisms for the two catalysts. FeOOH-NiOOH operates by a bifunctional mechanism where the rate-determining O-O bond forming step is the concerted OH^- attack on a Fe=O coupled with a hydrogen atom transfer to a Ni^{III}-O site. On the contrary, NiFe LDH operates by a conventional mechanism of four consecutive PCET steps, and the rate-determining O-O bond forming step is the attack of OH^- on a Fe=O unit.

The data describe here constitute the first experimental evidences for the bifunctional mechanism which has hitherto only computational supports. The superior activity of FeOOH-NiOOH demonstrates the potential of bifunctional catalysts to overcome the performance limit of conventional catalysts imposed by the scaling relationship. The bifunctional mechanism provide an opportunity to individually fine-tune two components of an OER catalyst for optimized activity, adding a new design principle. For example, analogous to the present FeOOH-NiOOH catalyst, the FeOOH component might be replaced by another material with a low energy barrier to form an electrophilic M=O unit, while the

NiOOH component might be replaced by another hydrogen atom acceptor, including even organic materials.

Acknowledgements

This work is supported by the European Research Council (No. 681292) and the Marie Skłodowska-Curie Fellowship (no. 838367) under the European Union's Horizon 2020 research. We thank Dr. Natalia Gasilova (EPFL) for ICP-AES measurements.

Conflicts of interests

The authors declare no competing financial interest.

Keywords: oxygen evolution reaction • electrokinetics • Raman spectroscopy • reaction mechanisms • nickel iron oxide

References

[1] (a) Z. W. Seh, J. Kibsgaard, C. F. Dickens, I. Chorkendorff, J. K. Norskov, T. F. Jaramillo, *Science* **2017**, *355*; (b) N. S. Lewis, *Science* **2016**, *351*, aad1920.

[2] (a) F. Song, L. Bai, A. Moysiadou, S. Lee, C. Hu, L. Liardet, X. Hu, *J Am Chem Soc* **2018**, *140*, 7748-7759; (b) B. M. Hunter, H. B. Gray, A. M. Muller, *Chem Rev* **2016**, *116*, 14120-14136; (c) N. T. Suen, S. F. Hung, Q. Quan, N. Zhang, Y. J. Xu, H. M. Chen, *Chem Soc Rev* **2017**, *46*, 337-365.

[3] (a) H. Dau, C. Limberg, T. Reier, M. Risch, S. Roggan, P. Strasser, *ChemCatChem* **2010**, *2*, 724-761; (b) C. Hu, L. Zhang, J. Gong, *Energy Environ Sci* **2019**, *12*, 2620-2645.

[4] I. C. Man, H.-Y. Su, F. Calle-Vallejo, H. A. Hansen, J. I. Martínez, N. G. Inoglu, J. Kitchin, T. F. Jaramillo, J. K. Nørskov, J. Rossmeisl, *ChemCatChem* **2011**, *3*, 1159-1165.

[5] M. T. M. Koper, *J Electroanal Chem* **2011**, *660*, 254-260.

[6] (a) M. Busch, *Curr Opin Electrochem* **2018**, *9*, 278-284; (b) M. Busch, N. B. Halck, U. I. Kramm, S. Siahrostami, P. Krtil, J. Rossmeisl, *Nano Energy* **2016**, *29*, 126-135.

[7] (a) M. Bajdich, M. Garcia-Mota, A. Vojvodic, J. K. Norskov, A. T. Bell, *J Am Chem Soc* **2013**, *135*, 13521-13530; (b) L.-P. Wang, T. Van Voorhis, *J Phy Chem Lett* **2011**, *2*, 2200-2204.

[8] (a) D. K. Bediako, Y. Surendranath, D. G. Nocera, *J Am Chem Soc* **2013**, *135*, 3662-3674; (b) A. Moysiadou, S. Lee, C. S. Hsu, H. M. Chen, X. Hu, *J Am Chem Soc* **2020**, *142*, 11901-11914; (c) Y. Surendranath, M. W. Kanan, D. G. Nocera, *J Am Chem Soc* **2010**, *132*, 16501-16509.

[9] (a) N. B. Halck, V. Petrykin, P. Krtil, J. Rossmeisl, *Phys Chem Chem Phys* **2014**, *16*, 13682-13688; (b) J. M. P. Martirez, E. A. Carter, *J Am Chem Soc* **2019**, *141*, 693-705; (c) F. Song, M. M. Busch, B. Lassalle-Kaiser, C.-S. Hsu, E. Petkucheva, M. Bensimon, H. M. Chen, C. Corminboeuf, X. Hu, *ACS Cent. Sci.* **2019**, *5*, 558-568.

[10] (a) L. Trotochaud, S. L. Young, J. K. Ranney, S. W. Boettcher, *J Am Chem Soc* **2014**, *136*, 6744-6753; (b) M. B. Stevens, C. D. M. Trang, L. J. Enman, J. Deng, S. W. Boettcher, *J Am Chem Soc* **2017**, *139*, 11361-11364; (c) S. Klaus, Y. Cai, M. W. Louie, L. Trotochaud, A. T. Bell, *J Phy Chem C* **2015**, *119*, 7243-7254.

[11] D. Friebel, M. W. Louie, M. Bajdich, K. E. Sanwald, Y. Cai, A. M. Wise, M. J. Cheng, D. Sokaras, T. C. Weng, R. Alonso-Mori, R. C. Davis, J. R. Bargar, J. K. Norskov, A. Nilsson, A. T. Bell, *J Am Chem Soc* **2015**, *137*, 1305-1313.

[12] (a) O. Diaz-Morales, I. Ledezma-Yanez, M. T. M. Koper, F. Calle-Vallejo, *ACS Catal* **2015**, *5*, 5380-5387; (b) Y.-F. Li, A. Selloni, *ACS Catal* **2014**, *4*, 1148-1153.

[13] X. Xu, F. Song, X. Hu, *Nat Commun* **2016**, *7*, 12324.

[14] D. Fu, P. G. Keech, X. Sun, J. C. Wren, *Phys Chem Chem Phys* **2011**, *13*, 18523-18529.

[15] (a) L. Francas, S. Corby, S. Selim, D. Lee, C. A. Mesa, R. Godin, E. Pastor, I. E. L. Stephens, K. S. Choi, J. R. Durrant, *Nat Commun* **2019**, *10*, 5208; (b) L. A. Stern, X. Hu, *Faraday discussions* **2014**, *176*, 363-379.

[16] (a) J. Chen, F. Zheng, S.-J. Zhang, A. Fisher, Y. Zhou, Z. Wang, Y. Li, B.-B. Xu, J.-T. Li, S.-G. Sun, *ACS Catal* **2018**, *8*, 11342-11351; (b) H. Yin, L. Jiang, P. Liu, M. Al-Mamun, Y. Wang, Y. L. Zhong, H. Yang, D. Wang, Z. Tang, H. Zhao, *Nano Research* **2018**, *11*, 3959-3971.

[17] (a) S. Lee, L. Bai, X. Hu, *Angew Chem Int Ed* **2020**, *59*, 8072-8077; (b) S. Lee, K. Banjac, M. Lingenfelder, X. Hu, *Angew Chem Int Ed* **2019**, *58*, 10295-10299; (c) B. J. Trzesniewski, O. Diaz-Morales, D. A. Vermaas, A. Longo, W. Bras, M. T. Koper, W. A. Smith, *J Am Chem Soc* **2015**, *137*, 15112-15121; (d) M. W. Louie, A. T. Bell, *J Am Chem Soc* **2013**, *135*, 12329-12337.

[18] O. Diaz-Morales, D. Ferrus-Suspedra, M. T. M. Koper, *Chem Sci* **2016**, *7*, 2639-2645.

[19] S. Zou, M. S. Burke, M. G. Kast, J. Fan, N. Danilovic, S. W. Boettcher, *Chem Mater* **2015**, *27*, 8011-8020.

[20] Z. Lu, W. Xu, W. Zhu, Q. Yang, X. Lei, J. Liu, Y. Li, X. Sun, X. Duan, *Chem Commun* **2014**, *50*, 6479-6482.

[21] (a) J. O. M. Bockris, *J Chem Phy* **1956**, *24*, 817-827; (b) M. E. G. Lyons, M. P. Brandon, *J Electroanal Chem* **2010**, *641*, 119-130.

[22] Y.-H. Fang, Z.-P. Liu, *ACS Catal* **2014**, *4*, 4364-4376.

[23] (a) H. Vrubel, T. Moehl, M. Gratzel, X. Hu, *Chem Commun* **2013**, *49*, 8985-8987; (b) D. Y. Chung, S. Park, P. P. Lopes, V. R. Stamenkovic, Y.-E. Sung, N. M. Markovic, D. Strmcnik, *ACS Catal* **2020**, *10*, 4990-4996.

[24] (a) A. C. Garcia, T. Touzalin, C. Nieuwland, N. Perini, M. T. M. Koper, *Angew Chem Int Ed* **2019**, *58*, 12999-13003; (b) J. D. Michael, E. L. Demeter, S. M. Illes, Q. Fan, J. R. Boes, J. R. Kitchin, *J Phy Chem C* **2015**, *119*, 11475-11481; (c) J. Zaffran, M. B. Stevens, C. D. M. Trang, M. Nagli, M. Shehadeh, S. W. Boettcher, M. Caspary Toroker, *Chem Mater* **2017**, *29*, 4761-4767.

[25] (a) G. Parkin, *Acc Chem Res* **2009**, *42*, 315-325; (b) W. Zhang, I. J. Burgess, *J Electroanal Chem* **2012**, *668*, 66-72.

[26] C. Pasquini, I. Zaharieva, D. Gonzalez-Flores, P. Chernev, M. R. Mohammadi, L. Guidoni, R. D. L. Smith, H. Dau, *J Am Chem Soc* **2019**, *141*, 2938-2948.

[27] (a) K. Sakaushi, *Phys Chem Chem Phys* **2020**, *22*, 11219-11243; (b) L. I. Krishtalik, *Biochimica et Biophysica Acta (BBA) - Bioenergetics* **2000**, *1458*, 6-27.

[28] M. Gómez-Gallego, M. A. Sierra, *Chem Rev* **2011**, *111*, 4857-4963.

[29] Y. Zhang, H. Zhang, H. Ji, W. Ma, C. Chen, J. Zhao, *J Am Chem Soc* **2016**, *138*, 2705-2711.

[30] (a) Y. Liu, C. C. L. McCrory, *Nat Commun* **2019**, *10*, 1683; (b) W. Li, F. Li, H. Yang, X. Wu, P. Zhang, Y. Shan, L. Sun, *Nat Commun* **2019**, *10*, 5074.

[31] N. Li, D. K. Bediako, R. G. Hadt, D. Hayes, T. J. Kempa, F. von Cube, D. C. Bell, L. X. Chen, D. G. Nocera, *Proc Natl Acad Sci USA* **2017**, *114*, 1486.

Entry for the Table of Contents

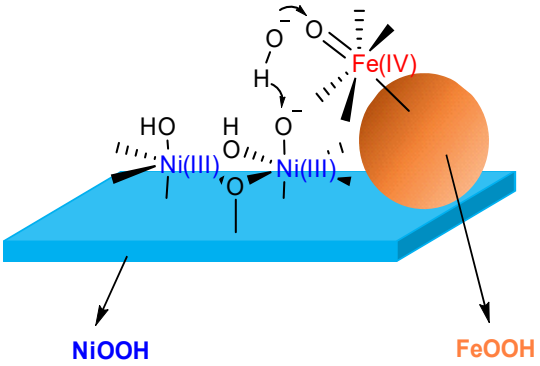

Operando Raman spectroscopic and electrokinetic study of two highly active OER catalysts, FeOOH-NiOOH and NiFe layered double hydroxide (LDH), was conducted. The data support two distinct mechanisms for the two catalysts: FeOOH-NiOOH operates by a bifunctional mechanism where the rate-determining O-O bond forming step is the OH- attack on an Fe=O coupled with a hydrogen atom transfer to a Ni^{III}-O site, whereas NiFe LDH operates by a conventional mechanism of four consecutive PCET steps.